Appl Phys A (2008) 93: 849–855
DOI 10.1007/s00339-008-4744-3

Applied Physics A
Materials Science & Processing

Cumulative and continuous laser vaporization synthesis of single wall carbon nanotubes and nanohorns

A.A. Puretzky · D.J. Styers-Barnett · C.M. Rouleau · H. Hu · B. Zhao · I.N. Ivanov · D.B. Geohegan

Received: 12 October 2007 / Accepted: 4 March 2008 / Published online: 28 June 2008
© Springer-Verlag 2008

Abstract The conditions for the scaled synthesis of single wall carbon nanotubes (SWNTs) and single wall carbon nanohorns (SWNHs) by laser vaporization at high temperatures are investigated and compared using in situ diagnostics. An industrial Nd:YAG laser (600 W, 1–500 Hz repetition rate) with tunable pulse widths (0.5–50 ms) is utilized to explore conditions for high-yield production. High-speed videography (50000 frames/s) of the laser plume and pyrometry of the target surface are correlated with ex situ high resolution transmission electron microscopy analysis of the products for pure carbon targets and carbon/catalyst targets to understand the effects of the processing conditions on the resulting nanostructures. Carbon is shown to self-assemble into single-wall nanohorn structures at rates of ∼1 nm/ms, which is comparable to the catalyst-assisted SWNT growth rates. Two regimes of laser ablation, *cumulative* ablation by multiple pulses and *continuous* ablation by individual pulses, were explored. Cumulative ablation with spatially overlapping 0.5-ms pulses is favorable for the high yield and production rate of SWNTs at ∼6 g/h while continuous ablation by individual long laser pulses (∼20 ms) at high temperatures results in the highest yield of SWNHs at ∼10 g/h. Adjustment of the laser pulse width is shown to control SWNH morphology.

PACS 79.20.Ds · 52.38.Mf · 81.07.De · 61.48.De

A.A. Puretzky (✉) · D.J. Styers-Barnett · C.M. Rouleau · H. Hu · B. Zhao · I.N. Ivanov · D.B. Geohegan
Oak Ridge National Laboratory, Oak Ridge, TN 37831-6056, USA
e-mail: puretzkya@ornl.gov

Pulsed laser ablation is a versatile technique for synthesis of many different nanomaterials including nanoparticles [1], nanowires [2], and nanotubes [3]. It was successfully used to produce single wall carbon nanotubes (SWNTs) with relatively narrow diameter distribution and low level of defects [3]. Typically, nanosecond laser pulses were used to produce SWNTs, although other pulse widths and laser ablation regimes were explored (see the review [4]).

Recently, we conducted extensive studies of the ns-laser ablation process of carbon targets containing ∼1 at.% of metal catalyst powders (Ni, Co) typically used for laser ablation synthesis of SWNTs at high temperatures (1100 °C) using in situ spectroscopic diagnostics and gated imaging techniques. It was shown that during the first 100 µs the laser ablation plumes consist mainly of atoms and molecules of carbon and metal. Within 1 ms following laser vaporization, carbon forms clusters as the hot plasma cools. Later in time metal catalysts form clusters (1 ms $< t <$ 2 ms after laser ablation) and carbon nanotubes grow inside the confined laser ablation plume over extended periods of time [5–7]. It was concluded that one of the main conditions to achieve a high yield of SWNTs was confinement of the ejected material inside the propagating laser plume and that the main mechanism of this confinement was formation of a vortex ring.

However, spreading the same laser energy over longer pulse widths was found to ablate similar quantities of material, yet with quite different plume confinement and improved nanotube yield. For example, Fig. 1 compares the plumes resulting from a Nd:YAG laser oscillating in both Q-switched and 'free-running' modes. As shown in Fig. 1, the plume volume is significantly reduced if a sequence of pulses with a relatively low peak power is used to ablate the target instead of individual ns-laser pulses with high peak power. A detailed study of this laser ablation regime revealed that preheating of the target with approximately ten laser pulses

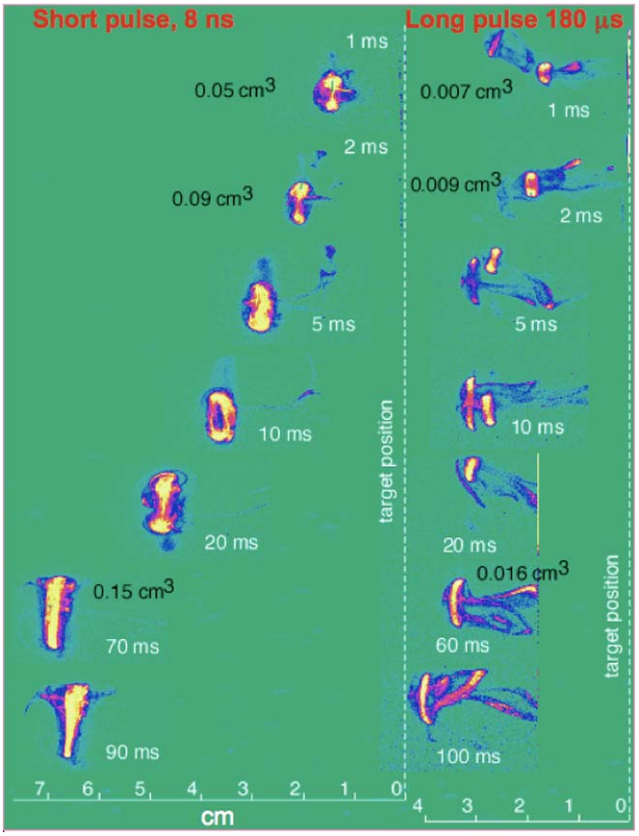

Fig. 1 Sequences of laser ablation plume images generated from a C/Ni/Co target into flowing Ar at 1150 °C using short (8 ns) Nd:YAG laser pulses (*left*) and long pulses (∼80 pulses, 300 ns and 5 $\times 10^4$ W peak power each, 180-µs total length, a free-running mode of a Nd:YAG laser) (*right*) with the same total energy of ∼350 mJ. The numbers in black show estimated plume volumes

was required to achieve stationary ablation. Weight analysis of the target and high resolution transmission electron microscopy (HRTEM) of the products revealed that, averaged over many pulses, the same ablation rates were achieved for the same total input energy between single-shot and multi-shot ablation, but higher conversion efficiencies of carbon to SWNTs were obtained when the ejected material was confined in a smaller volume. Therefore, this *cumulative* regime of laser ablation can be advantageous for the synthesis of SWNTs and other nanomaterials that rely upon long-term confinement and annealing of the ablated material.

Other interesting carbon nanostructures, including single wall carbon nanohorns (SWNHs), were discovered by Iijima et al. using high-power, long-pulse (5 kW, 0.5 s at 1 Hz) CO_2 laser vaporization of pure carbon in Ar at atmospheric pressure and room temperature [8]. Using this approach they were able to produce ∼10 g/h of SWNH aggregates with an average diameter ∼100 nm and to study their growth mechanisms using in situ imaging and spectroscopy [9]. Although some variation in the morphologies of SWNH aggregates was demonstrated using different background gases [10], it was not sufficient to control the structures of these aggregates using this approach. In addition, the long pulse CO_2 laser synthesis produced graphitic impurities [11].

In this paper, the synthesis efficiency and morphologies of both SWNTs and single wall carbon nanohorns (SWNHs) are reported resulting from different regimes of laser ablation. For this purpose, a high power (600 W) industrial Nd:YAG laser (JK760TR, GSI Lumonics) with tunable pulse widths was employed in conjunction with in situ high-speed videography and pyrometry of the target surface. It was demonstrated that *cumulative* laser ablation gives a relatively high yield and high production rate of SWNTs (∼6 g/h) and that *continuous* laser ablation by individual long laser pulses (∼10 ms) at high temperature results in synthesis of SWNHs (∼10 g/h). In the latter case control over the morphologies of SWNHs is reported, which depends upon the width of the laser pulse.

1 Experimental

The experimental setup was similar to that described in [6]. It included a quartz tube (3-in. diameter, 48-in. length) mounted inside a hinged tube furnace (Lindberg Blue) operating at 1150 °C. The ends of the quartz tube were O-ring-sealed in vacuum flanges and the entire system was evacuated by a mechanical pump to control the growth environment. Argon was introduced around the laser entrance window to maintain specified pressures and flow rates to carry the nanomaterials out of the furnace into a collection chamber fitted with a HEPA filter. The growth reactor was equipped with a fast sampling unit that allowed collecting SWNT and SWNH samples during synthesis for scanning electron microscopy (SEM), TEM, and optical spectroscopy characterization. The Nd:YAG ($\lambda = 1.064$ µm) laser light was delivered through a 0.6-mm-diameter fiber optic cable and focused through an anti-reflection-coated window onto a target positioned in the center of the furnace. The collimating ($f = 20$ cm) and focusing ($f = 1$ m) lenses were mounted on a robotic arm (IX SCARA Robot, IAI Inc.) and can be moved to scan the laser beam (4-mm spot diameter) across a target in predesigned raster patterns to achieve uniform target erosion during long time synthesis scans. The main laser parameters are listed in Table 1. The maximum peak power of 10 kW could not be maintained at all pulse widths because of the limitation on the maximum energy per pulse. Similarly, the maximum repetition rate could not be used for all pulse energies due to the limitation on the maximum average power. The set of the available laser parameters is shown in Fig. 2a. For example, it can be seen that the maximum peak power stays at 10 kW only for pulse widths $t_p \leq 10$ ms and decreases as $100/t_p$ (kW) for $t_p \geq 10$ ms, where t_p is in ms (Fig. 2a). The repetition rate of 500 Hz

Table 1 Parameters of the high-power Nd:YAG laser

Wavelength	Maximum peak power	Maximum energy/pulse	Pulse width	Maximum repetition rate	Maximum average power
1.064 µm	10 kW	100 J	0.5–50 ms	500 Hz	600 W

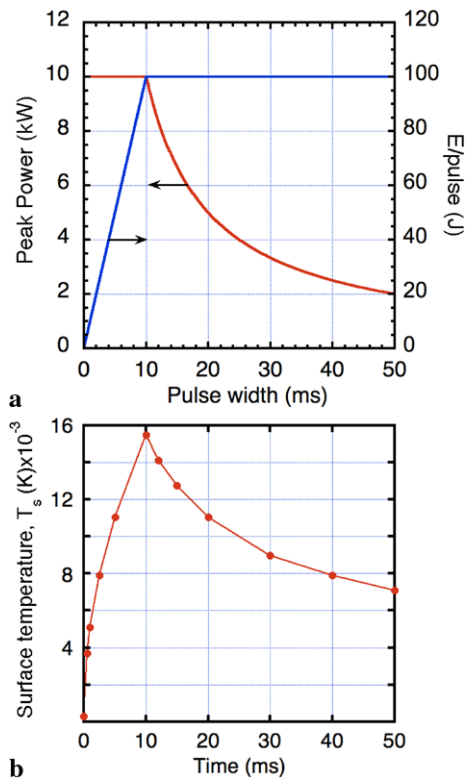

Fig. 2 (**a**) The peak power and energy per pulse vs. pulse width; (**b**) the surface temperature of a graphite target estimated according to (1) using peak power, $I_p(t_p)$, shown in (**a**)

could be maintained only at energies per pulse $E_p \leq 1.2$ J and dropped as $600/E_p$ (Hz) at $E_p \geq 1.2$ J, where E_p is in J.

The amount of ablated material is defined by the surface temperature, T_s, that in the 1D approximation can be estimated as

$$T_s = T_0 + 2I\left(\frac{t_p}{\pi k \rho c_p}\right)^{1/2}, \tag{1}$$

where T_0 is the initial temperature, $I = I_p/\pi R^2$, I_p is the laser peak power, R is the radius of the laser beam spot, and $k = 500$ W/mK, $\rho = 1400$ kg/m^3, and $c_p = 500$ J/kg K are the thermal conductivity, density, and specific heat capacity of the carbon target, respectively. Although (1) overestimates the values of the surface temperatures since it does not take into account the heat of evaporation, it gives a qualitative estimate of the effectiveness of laser ablation for a particular set of the laser parameters. For example, it can be

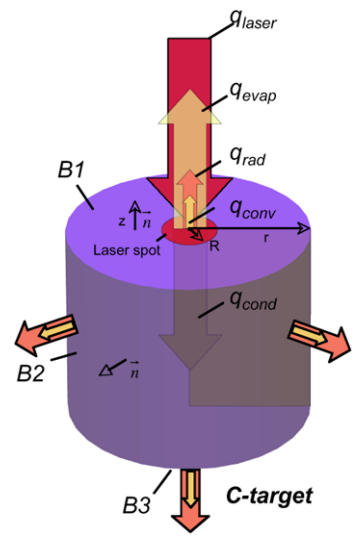

Fig. 3 Boundary heat fluxes for the considered 3D model of laser heating of a graphite target

seen that the most effective ablation yield can be achieved using 10-ms laser pulses for the laser used in this study (Fig. 2b).

2 3D model of heat transfer

To understand different regimes of laser ablation and to explore the cumulative laser ablation for synthesis of SWNTs and SWNHs, we developed a 3D model that includes heating with a laser beam, heat losses due to heat conduction, target evaporation, black-body radiation, and cooling by the surrounding buffer gas using the heat-transfer module of the Comsol software. The following expressions were used to estimate the heat fluxes at the boundaries B1, B2, and B3 of a carbon target (1-in. diameter and 1-in. height) shown in Fig. 3:

$$\begin{aligned} q_{\text{laser}} &= \frac{I_0(t)}{\pi R^2} e^{-\frac{r^2}{R^2}}, \qquad q_{\text{evap}} = A T^{-\frac{1}{2}} e^{-E/T}, \\ q_{\text{rad}} &= \varepsilon\sigma\left(T_{\text{amb}}^4 - T^4\right), \qquad q_{\text{conv}} = h(T_{\text{amb}} - T), \\ q_{\text{cond}} &= -\vec{n} \cdot (-k\nabla T), \end{aligned} \tag{2}$$

where q_{laser}, q_{evap}, q_{rad}, q_{conv}, and q_{cond} are the laser power density, the evaporation, the radiative, the convective, and the conductive heat fluxes, respectively, $I_0(t)$ is the laser peak power [W], T is the temperature, A is a constant, E

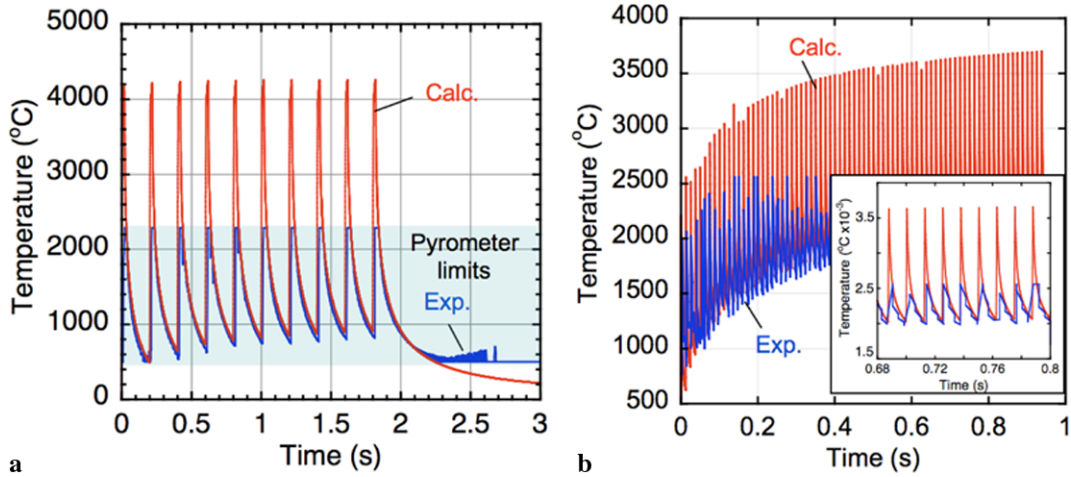

Fig. 4 Calculated and measured temperatures in the center of laser spot at $r = 0$ vs. time (**a**) for irradiation with long laser pulses (20 ms, 100 J/pulse) at 5 Hz and (**b**) short pulses (0.5 ms, 5 J/pulse) at 80 Hz. The *highlighted horizontal band* in (**a**) shows the pyrometer limits

is the heat of evaporation, ε is the emissivity, $\sigma = 5.67 \times 10^{-8}$ W/m^2 K^4 is the Stefan–Boltzmann constant, T_{amb} is the ambient temperature [K], and h is the convective heat transfer coefficient [W/m^2 K].

Figure 4a, b show the calculated and measured temperatures in the center of the laser ablation spot ($r = 0$, Fig. 3) vs. time for two different cases: ablation by 'long' and 'short' laser pulses: 20 ms, 100 J/pulse, 5 Hz and 0.5 ms, 5 J/pulse, 80 Hz, respectively. The temperature range for the experimental curves was limited by the temperature limits of the fast (~2-ms response time) pyrometer used for these measurements (Fig. 4a).

These examples demonstrate two different regimes of laser ablation of graphite targets, i.e. *continuous* ablation by individual laser pulses (Fig. 4a) and *cumulative* ablation when the preheating of a target by initial laser pulses is required to achieve the stationary ablation (Fig. 4b). In the first case (Fig. 4a) temperatures as high as 4200 °C can be achieved at the end of a 20-ms laser pulse that corresponds to the saturated vapor pressure of graphite, P_{sat}, of ~76 Torr. In the second case (Fig. 4b) the initial laser pulses heat the target up to ~2500 °C and cannot produce any substantial evaporation of the graphite target ($P_{\text{sat}} \approx 3 \times 10^{-3}$ Torr), but later the temperature reaches the stationary value of ~3700 °C because of the preheating due to the initial laser pulses that leads to $P_{\text{sat}} \approx 15$ Torr. The fit to the experimental temperatures gives an estimate of the thermal conductivity (~25 W/mK) of the graphite target used in these experiments.

3 In situ imaging of plume dynamics

The cumulative regime of the ablation was also investigated using direct in situ imaging of the laser ablation plume and monitoring of the intensity of the black-body emission from the laser-irradiated spot on the surface of the graphite target. Figure 5 shows a set of the selected frames from a movie taken with a high-speed camera (10^4 frames/s, 67-μs gate width) during laser irradiation using 16 sequential pulses, 0.5 ms, 4.5 J/pulse, at 80 Hz. The selected frames show the results of the laser irradiation after 6 ms following each sequential laser pulse. These images show that the stationary laser ablation, i.e. well-developed plumes with approximately similar shapes and propagation dynamics, appear only after 11 or 12 laser pulses. The first laser pulses produce only small plumes located close to the target surface. The brightness of the laser spot at the target surface that is directly related to the temperature inside the irradiated area also increases and saturates after approximately 11 or 12 laser pulses (Fig. 5), in good agreement with calculations (Fig. 4b).

Figure 6 compares plume dynamics measured for two different cases, 'short' (1 ms, 9.0 J) and 'long' (10 ms, 90.4 J) laser pulses. In the first case (Fig. 6a) the ejected material is well confined in a relatively small vortex ring after the end of the laser pulse (2-ms frame, Fig. 6a). In the second case (Fig. 6b) the plume dynamics is completely different and the different parts of the plume have completely different temperatures. For example, it can be seen that at 7 ms after the beginning of the laser pulse some material escaped from the plume and cooled down rapidly because of the weak interaction with the main hot plume (the black smoke at the top left corner). The different plume dynamics provides completely different environmental conditions for synthesis of nanomaterials using laser ablation. For example, synthesis of carbon nanotubes requires a composite carbon target containing small amounts of metal catalyst. To nucleate the growth of SWNTs the catalyst and carbon should be confined within the same volume during

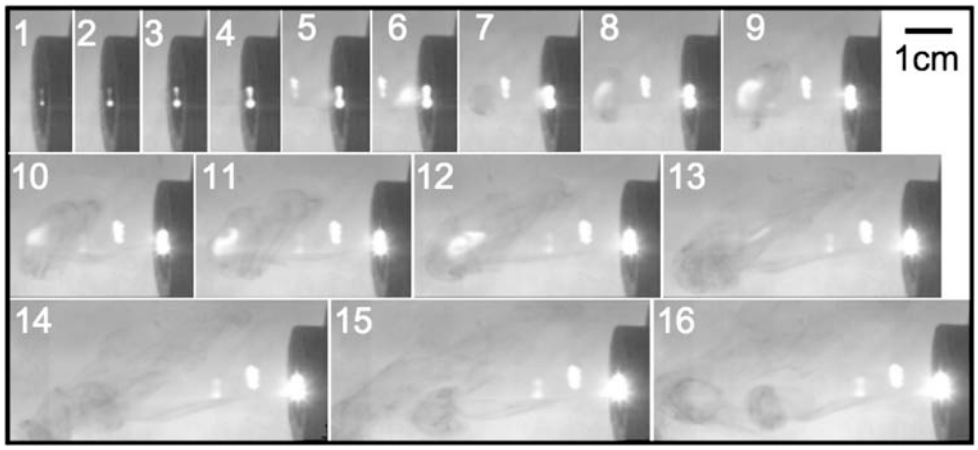

Fig. 5 Sequence of images taken during laser irradiation of graphite target using 0.5 ms, 4.5 J/pulse laser pulses at 80 Hz. The irradiation was conducted at room temperature in 500 Torr of flowing Ar (1000 sccm flow rate)

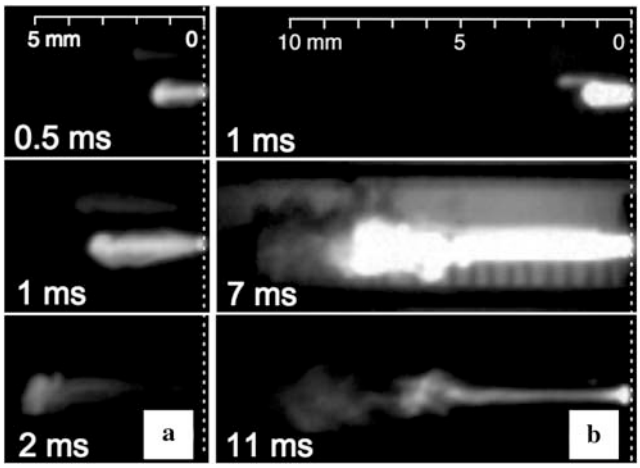

Fig. 6 Images of plume dynamics measured using two different laser pulses, (**a**) 1 ms, 9.0 J and (**b**) 10 ms, 90.4 J at 1100 °C in flowing Ar (1000 sccm, 760 Torr) taken with a fast camera (5×10^4 frames/s, 1-μs and 5-μs gate widths), respectively

and after the laser ablation pulse. Additionally, the efficient growth of carbon nanotubes requires confinement of the catalyst and carbon feedstock species for a relatively long time [5–7]. The 'short' pulse plume dynamics better satisfies the confinement requirement. Synthesis of single wall carbon nanohorns utilizes a pure graphite target and occurs on the millisecond time scale when the plume is still relatively hot. In this case the main requirements for the efficient synthesis are the high concentration and the high temperatures of the ejected species.

4 Growth rates, morphologies, and production rates of SWNHs

Figure 7 shows TEM images of SWNHs synthesized at the optimized conditions using 20-ms laser pulses at a low laser pulse repetition rate of 5 Hz and 0.5-ms pulses at 80 Hz. Interestingly, the laser ablation of pure graphite targets at high temperatures produces high yields of SWNHs. That raises the following questions: (1) how can high-power laser vaporization produce single wall carbon nanohorns in such high yields without a catalyst? (2) Is there a common precursor (e.g. fullerenes) for both nanohorn and nanotube growth by laser vaporization? (3) What are the temporal and spatial scales for growth? To address these questions, we conducted detailed in situ imaging of the plume dynamics generated from pure graphite targets by the laser pulses with variable durations from 0.5 ms to 20 ms and combined this data with ex situ TEM and SEM characterization of SWNHs synthesized at these conditions. The detailed analysis of these data will be published elsewhere.

Here, we briefly summarize the main results of this study. First, comparing the relative intensities of the black-body emission from the internal furnace wall and from the laser ablation plumes we estimated that ∼6 and 23 ms are required for the species within the propagating plumes to cool down to the furnace temperature of 1150 °C for 0.5- and 20-ms laser pulses, respectively. Since the length of the individual nanohorn units synthesized at these pulse lengths (estimated from the corresponding TEM images) varies from ∼10 to 30 nm, it is possible to obtain a rough estimate of the SWNH growth rate as ∼1 nm/ms, which is comparable to the growth rate of SWNTs [7]. Second, different laser pulses produce SWNHs with different average sizes and morphologies, i.e. the shorter the pulse the smaller and smoother the SWNH aggregates it generates (Fig. 7). Larger diameter aggregates with the sharp conical shape of the individual SWNH units can be produced using a 20-ms laser pulse (Fig. 7). The size distribution of SWNHs was also measured in situ using a differential mobility analyzer (DMA) [12]. Third, the interstitial spacing between the individual units also depends on the length of the laser pulse. The shortest pulses lead to the most compact packing of the individual units with the smallest interstitial spacing.

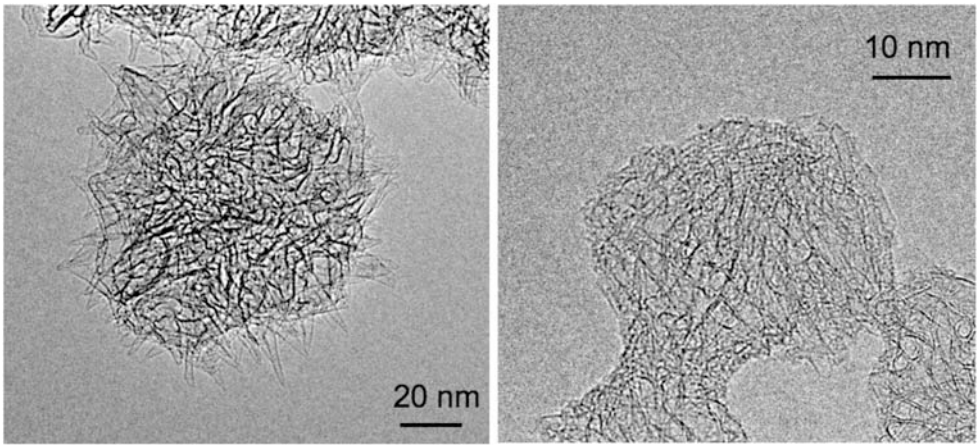

Fig. 7 TEM images of SWNHs synthesized using 20-ms, 5-Hz repetition rate (*left*) and 0.5-ms, 80-Hz laser pulses (*right*)

Although the mechanism of formation of individual SWNH units and their assembly into different morphology spherical aggregates is not understood yet, our preliminary results based on in situ DMA measurements demonstrate the possibility of sublimation of small particles with the mobility diameters of 15–20 nm from the nanohorn soot at temperatures >950 °C [12]. This indicates that one of the possible scenarios of SWNH growth is the formation of individual units followed by their self-assembly into spherical aggregates. The size and morphology of the individual units depend on the ablation conditions, i.e. the initial concentration of the carbon species, and their temperatures in the laser ablation plumes. The shorter laser pulses generate a laser ablation plume with a smaller initial concentration of carbon species that cools down faster compared to that produced by longer laser pulses. This restricts the growth time of the individual nanohorns and results in synthesis of smaller units. The smaller nanohorn units have an elongated fullerene-type shape and a relatively narrow size distribution that leads to more compact assembly of the individual units into SWNH aggregates.

To estimate the production rates of SWNHs and SWNTs, the ablated material from the collection chamber and the quartz tube was collected and weighed. The production rates, 10 g/h for SWNHs and 6 g/h for SWNTs, were estimated as the ratio of this weight to the total time when the laser was running. It was found that the total ablation rate, estimated as the difference of the target weights before and after ablation per total ablation time, was approximately 10% higher than the corresponding production rates, indicating that the collection efficiency of the setup is ∼90%.

5 Conclusions

In summary, we explored two regimes of laser ablation for synthesis of SWNTs and SWNHs using a high-power Nd:YAG laser with variable pulse width: *continuous* ablation that provides sustained temperatures sufficient for self-organization of the ablated species into single wall carbon nanostructures (SWNHs) and *cumulative* ablation which is optimal for the growth of SWNTs with catalyst assistance. However, when using catalyst assistance it was observed that conditions exist for simultaneous production of SWNTs and SWNHs, which indicates competitive kinetics between catalyst-assisted and catalyst-free growth pathways for single wall carbon nanostructures. Diagnostics and ex situ analysis show that carbon can self-assemble into single wall nanohorn structures at rates of ∼1 nm/ms, which is comparable to the catalyst-assisted SWNT growth rates measured previously [7]. A 3D model of heat transfer in the ablation targets with a moving laser beam was developed to determine the thermal conductivity of the ablation targets, optimize the ablation yield in cumulative laser ablation, and achieve uniform target erosion during a synthesis run. Based on these studies we were able to develop an efficient laser ablation approach and apparatus for the synthesis of relatively large amounts of SWNTs and SWNHs with high production rates of ∼6 and 10 g/h, respectively. According to theoretical predictions, SWNHs are a promising material for hydrogen storage applications [13]. The ability to synthesize high yields of pure SWNHs with different morphologies permits the exploration of these materials with tunable porosity for hydrogen storage. The results of this study will be published elsewhere.

Acknowledgements Synthesis science on carbon nanostructure growth by laser vaporization and CVD [AP, DG, CR] was funded by the Division of Materials Sciences and Engineering, Office of Basic Energy Sciences at DOE. Characterization of SWNHs and SWNTs [HH] was funded by the EERE Center of Excellence on Carbon-Based Hydrogen Storage, Office of Energy Efficiency and Renewable Energy, and independent research [BZ, II, DSB] at the Center for Nanophase Materials Sciences, Division of Scientific User Facilities, DOE. Oak Ridge National Laboratory is operated under the management of UT-Battelle, LLC for the US Department of Energy under Contract No. DE-AC05-00OR22725.

References

1. D.B. Geohegan, A.A. Puretzky, G. Duscher, S.J. Pennycook, Appl. Phys. Lett. **72**, 2987 (1998)
2. A.M. Morales, C.M. Lieber, Science **279**, 208 (1998)
3. T. Guo, P. Nikolaev, A. Thess, D.T. Colbert, R.E. Smalley, Chem. Phys. Lett. **243**, 49 (1995)
4. C.T. Kingston, B. Simard, J. Nanosci. Nanotechnol. **6**, 1225 (2006)
5. A.A. Puretzky, D.B. Geohegan, X. Fan, S.J. Pennycook, Appl. Phys. Lett. **76**, 182 (2000)
6. A.A. Puretzky, D.B. Geohegan, X. Fan, S.J. Pennycook, Appl. Phys. A **70**, 153 (2000)
7. A.A. Puretzky, H. Schittenhelm, X. Fan, M.J. Lance, L.F. Allard Jr., D.B. Geohegan. Phys. Rev. B **65**, 245425 (2002)
8. S. Iijima, M. Yudasaka, R. Yamada, S. Bandow, K. Suenaga, F. Kokai, K. Takahashi, Chem. Phys. Lett. **309**, 165 (1999)
9. F. Kokai, K. Takahashia, D. Kasuya, M. Yudasaka, S. Iijima, Appl. Surf. Sci. **197–198**, 650 (2002)
10. D. Kasuya, M. Yudasaka, K. Takahashi, F. Kokai, S. Iijima, J. Phys. Chem. B **106**, 4947 (2002)
11. J. Fan, M. Yudasaka, D. Kasuya, T. Azami, R. Yuge, H. Imai, Y. Kubo, S. Iijima, J. Phys. Chem. B **109**, 10756 (2005)
12. M.D. Cheng, D.W. Lee, B. Zhao, H. Hu, D.J. Styers-Barnett, A.A. Puretzky, D.W. DePaoli, D.B. Geohegan, E.A. Ford, P. Angelini, Nanotechnology **18**, 185604 (2007)
13. F. Fernandez-Alonso, F.J. Bermejo, C. Cabrillo, R.O. Loutfy, V. Leon, M.L. Saboungi, Phys. Rev. Lett. **98**, 215503 (2007)